
Applications of Carbon Nanotubes to Flexible Transparent Conductive Electrodes

Bu-Jong Kim and Jin-Seok Park

Additional information is available at the end of the chapter

<http://dx.doi.org/10.5772/intechopen.72002>

Abstract

Transparent conductive electrodes (TCEs) have attracted great interest because of their wide range of applications in solar cells, liquid crystal displays (LCDs), organic light-emitting diodes (OLEDs), and touch screen panels (TSPs). Indium-tin-oxide (ITO) thin films as TCEs possess exceptional optoelectronic properties, but they have several disadvantages such as a brittle nature due to their low fracture strain and lack of flexibility, a high processing temperature that damages the flexible substrates, low adhesion to polymeric materials, and relative rarity on Earth, which makes their price unstable. This has motivated several research studies of late for developing alternative materials to replace ITO such as metal meshes, metal nanowires, conductive polymers, graphene, and carbon nanotubes (CNTs). Out of the abovementioned candidates, CNTs have advantages in chemical stability, thermal conductivity, mechanical strength, and flexibility. However, there are still several problems yet to be solved for achieving CNT-based flexible TCEs with excellent characteristics and high stability. In this chapter, the properties of CNTs and their applications especially for flexible TCEs are presented, including the preparation details of CNTs based on solution processes, the surface modification of flexible substrates, and the various types of hybrid TCEs based on CNTs.

Keywords: carbon nanotubes, flexible transparent conductive electrodes, solution processes, hybrid-type electrodes, PEDOT:PSS, metal meshes, transmittance, reflectance, color properties

1. Introduction

Transparent conductive electrodes (TCEs) are thin films of optically transparent and electrically conductive materials. Indium tin oxide (ITO) has been the most widely used TCEs in rigid electronics due to its exceptional electrical and optical properties. Recently, flexible

TCEs fabricated by solution processes, which have some advantages such as simple and continuous process and relatively low costs, have attracted enormous interest because of their wide range of applications in flexible devices such as displays, touch screen panels (TSPs), sensors, film heaters that can attach to the skin, fabrics, and papers [1, 2]. However, ITO has disadvantages in the application fields where flexibility is ensured due to its brittle nature because of its low fracture strain and absence of flexibility, a high processing temperature that damages the flexible substrates, low adhesion to polymeric materials, and their relative rarity on Earth, which makes their price unstable [3]. Therefore, this has recently motivated various researches to discover alternative materials to replace ITO films, which include metal meshes, silver nanowires, conductive polymers, graphene, and carbon nanotubes (CNTs) [4, 5]. Also, for the flexible applications, the TCEs are required to be deposited on polymer substrates such as polyethylene terephthalate (PET), polypropylene (PP), and polydimethylsiloxane (PDMS).

Metal meshes and nanowires have excellent electrical properties, but they also have some problems such as visibility due to the reflectivity of metals and reliability for oxidation of metals [6]. Additionally, for metal nanowires, high contact resistances between individual nanowires have critical issues [7]. The conductive polymers, graphene, and CNTs have great advantages such as high mechanical flexibility and low processing costs because they can utilize solution processes [8]. Conductive polymers, however, are generally known to be not good enough at stability in an ambient atmosphere. Also, the poly(3, 4-ethylene-dioxythiophene):poly(styrenesulfonate) (PEDOT:PSS), which may be the most widely used conductive polymers, is tinged with the color blue, which may cause the problem of patterns of electrodes being revealed in TSPs [9]. Graphene has also been reported to be synthesized using solution processes such as the chemical reduction of exfoliated graphite oxide [10]. However, a thermal treatment at high temperature is needed for achieving high transparency and conductivity of graphene, which may restrict the use of flexible substrates.

CNTs, which have potential in chemical stability, thermal and electrical conductivity, mechanical strength, and flexibility, may be the best alternative material for applications in flexible TCEs. Actually, CNTs in some applications, which have low conductivity regardless of transmittance, are being commercialized. The rough surface of CNT films due to their tubular structures brings about a serious problem in the application of organic light-emitting diodes (OLEDs) [11]. In CNTs, furthermore, a relatively high contact resistance of the tube-tube junction may lead to insufficient sheet resistance [12]. Regarding this issue, the separation method of metallic and semiconducting components in CNTs by controlling the diameter and chirality of CNTs has been introduced in the literature [13]. The perfect separation technology, however, has not been realized yet as such a process is very complex. In addition, the chemical doping technology that lowers the sheet resistance has been introduced [14], but effectively controlling the defects in the CNTs is still difficult. As another method of improving the electric characteristics of CNTs, studies on the manufacturing of hybrid-type transparent electrodes have been attempted by several research groups.

In this chapter, the properties of CNTs and their applications especially for flexible TCEs are presented. First, the preparation details of CNTs based on solution processes are introduced, including purification and dispersion of CNT suspension, spray coating of CNTs,

and posttreatment of CNTs. Then, the surface modification of flexible substrates for enhancing the adhesion between CNTs and flexible substrates, which can eventually improve the flexibility of CNT-based TCEs, is discussed. Also, the effects of PEDOT:PSS coating on the electrical characteristics and color properties (e.g., redness, yellowness) of CNT-based TCEs are described, where the various methods for PEDOT:PSS coating, such as spin coating and electrophoretic deposition (EPD), are introduced and compared. Finally, the hybrid-type TCEs, which are fabricated by coating metal meshes with CNTs, are presented along with their characteristics as flexible TCEs.

2. Preparation of CNTs

2.1. Purification and dispersion of CNT suspension

Figure 1(a) shows the procedures for production of CNT suspension, including purification and dispersion processes. The synthesized CNTs necessarily contain metal catalyst and carbonaceous substances, including amorphous carbon, fullerenes, and graphite particles [15]. Therefore, to obtain high purity CNTs, the purification processes have to be conducted prior to the deposition of CNTs. Here, the chemical method induces the oxygenated functional group on CNTs, which causes damage to the surface of CNTs and eventually leads to an increase in the sheet resistance of CNTs. This indicates that it is important to determine the appropriate purification time when the chemical method is used.

After purification, the CNTs have to be properly dispersed since the van der Waals attraction forces between CNTs and the poor solubility of CNTs result in the formation of bundles and agglomerates [16]. There are several approaches for the dispersing of CNTs such as chemical modification (i.e., covalent approach), mechanical treatment, using of surfactants (i.e., noncovalent approach), and so on [17]. The chemical modification improves the solubility of CNTs

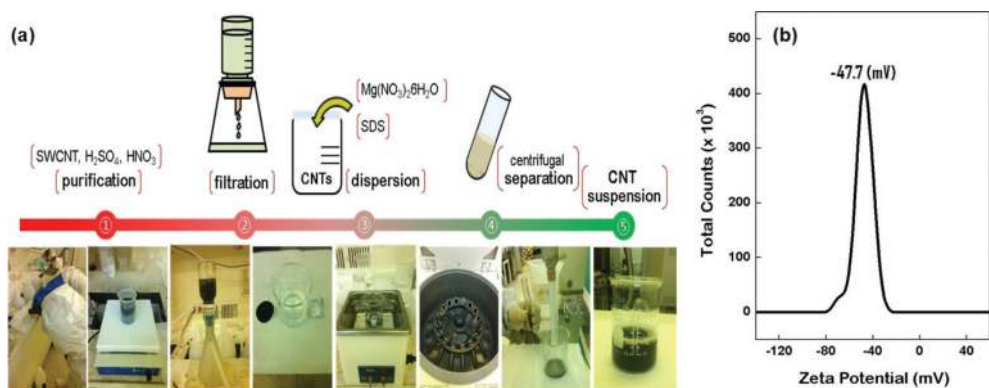


Figure 1. (a) The procedures for production of CNT suspension, including purification and dispersion processes and (b) the zeta potential measured from the prepared CNT suspension.

in solvent by attaching the various moieties and functional groups. However, the chemical method may also affect the electrical properties of CNTs. For the mechanical treatment, the applied high power can effectively separate CNTs, but it can also cause shortening of the CNTs.

In contrast to the chemical and mechanical approaches, the use of surfactants is based on the adsorption of chemical moieties onto the CNTs' surface without damaging the inherent properties of CNTs. Here, the dispersion method for achieving the stable CNT suspension using surfactant is introduced. The purified CNTs are filtered out using the vacuum filtering system, and the dispersion process is carried out for about 30 min in the ultrasonic generator after adding the anionic surfactant of sodium dodecyl sulfate (SDS, $\text{NaC}_{12}\text{H}_{25}\text{SO}_4$, 40 mg) together with deionized water (50 ml). Finally, only the dispersed supernatant is extracted by using the centrifugal separator with the speed of 4000 rpm for 30 min. The actual photo of the CNT suspension produced in this manner is also shown in **Figure 1(a)**. To confirm that the CNT suspension is well dispersed, the zeta potential of the CNT suspension is measured. Generally, the stable state of CNT suspension has a zeta potential of ± 40 mV or higher. **Figure 1(b)** shows the zeta potential measured with the CNT suspension of **Figure 1(a)** and it was about 47.7 mV, indicating that the CNT suspension was well dispersed.

2.2. Solution-based deposition of CNTs

Recently, solution-based processes have been increasingly adopted in the deposition of thin films since they have several advantages over the vacuum deposition system such as low fabrication cost, simple process, and massive scalability. To deposit CNTs on the flexible substrates, various methods have been developed, including spray coating, dip coating, bar coating, and inkjet printing [18, 19]. Among them, the spray coating method has the advantage that the thickness of deposited CNTs can be controlled precisely. Here, the CNT-TCEs, fabricated by depositing the CNTs on the polyethylene terephthalate (PET) substrates via spray coating, are presented. The process conditions are controlled by varying the spraying time from 10 to 80 s and by fixing the other process variables such as the injection pressure of 0.2 MPa, the injection amount of 2 ml/min, and the hotplate temperature of 100°C. **Figure 2(a)** indicates the schematic of the spray coating system used in this study and **Figure 2(b)** shows the photo of the surface morphology of CNTs, deposited on the PET substrate via spray coating, obtained using the field-emission scanning electron microscope (FE-SEM).

2.3. Posttreatment of CNTs

After the deposition of CNTs, the surfactant (e.g., SDS) may still remain in the CNTs and serves as an insulating layer, which may disturb the effective electrical contact of the CNTs. Therefore, the posttreatment for removing the remaining surfactant has to be conducted. Several posttreatment methods have been adopted to remove surfactants [20]. Here, the posttreatment of CNTs using nitric acid (HNO_3) is introduced. **Figure 3(a)** compares the sheet resistances and transmittances of CNTs before and after the HNO_3 posttreatment. After the HNO_3 posttreatment, the sheet resistance of CNTs was decreased. This was because the surfactant was removed. **Figure 3(b)** shows the change in the relative percentage of the chemical components incorporated in the CNTs due to the HNO_3 posttreatment, which was estimated

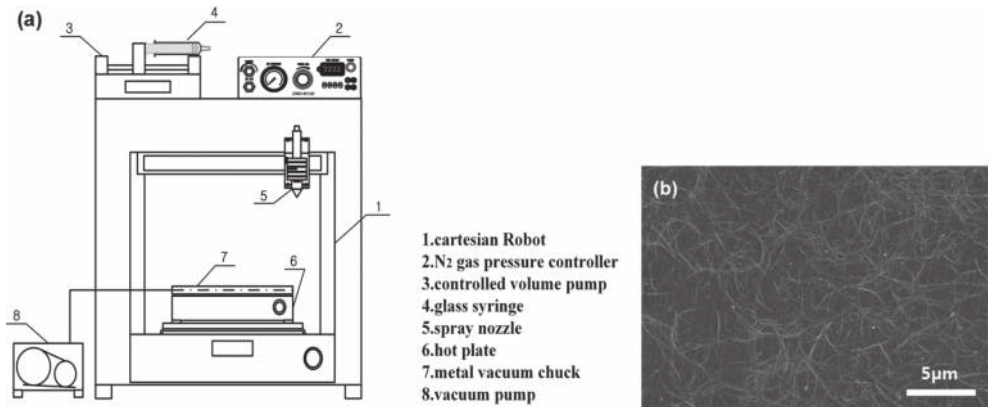


Figure 2. (a) The schematic of the spray coating system and (b) the FE-SEM image indicating the surface morphology of CNTs deposited on the PET substrate via spray coating.

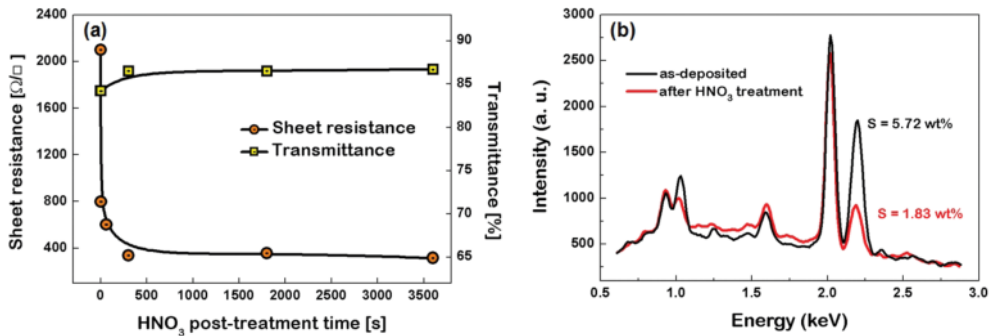


Figure 3. (a) The sheet resistances and transmittances of CNTs before and after HNO₃ posttreatment and (b) the EDS results indicating the change of the chemical components incorporated in the CNTs due to the HNO₃ posttreatment.

by using the energy dispersive X-ray spectroscopy (EDXS). The amount of sulfur (S) element in the CNTs was decreased after the HNO₃ posttreatment, which was resulted from the removal of the surfactant. Meanwhile, the transmittance of the CNTs slightly increased after the HNO₃ posttreatment, as also shown in **Figure 3(a)**. This was because some of the CNTs together with the surfactant were peeled off during the HNO₃ posttreatment.

3. CNT-TCEs fabricated on corona-treated flexible substrates

For depositing CNTs on flexible substrates, various solution-based methods have been utilized. However, these methods have common problems regarding the weak adhesion between the flexible substrates and the CNTs. Generally, the most widely used method is surface modification of substrate to improve the adhesion by using plasma treatment [21, 22]. This method

is a chemical modification that can be formed on polar groups on the surface of substrate before film deposition and also includes the physical changes, which can increase the surface area by generating nanoscratches. However, most of these methods have several problems such as low working pressures, long treatment times, and high processing temperatures. Therefore, corona pretreatment has also been suggested because it can be carried out at atmospheric pressure and room temperature. During the corona treatment, corona energy breaks molecular bonds on the surface of nonpolar substrates, and the broken bonds then recombine with free radicals in the corona environment to form polar groups on the film surface [23]. Namely, the surface of flexible substrate can be changed from hydrophobic to hydrophilic through the corona treatment.

In Section 3, the experimental results that regard the surface modification of PET substrates through corona treatment before the deposition of CNTs and the effects of such surface modification on the properties of the CNTs as flexible TCEs are presented. The changes in the surface roughness, contact angle, and surface energy of the PET substrates due to the corona treatment are characterized in terms of the applied corona energies, PET feeding directions, and treatment times.

3.1. Surface modification of PET substrates via corona treatment

For surface modification, the PET substrates were treated using corona discharge prior to the deposition of CNTs. **Figure 4(a)** shows the schematic of the corona discharge system. **Figure 4(b)** and **(c)** illustrates the corona treatment methods, including the feeding directions of the PET substrates and the numbers of treatment (e.g., 2-times and 4-times for the single-directional treatment and [1 + 1]-times and [2 + 2]-times for the mutually vertical bidirectional treatment). The corona discharge was generated by applying 8 kV voltage to the corona electrode. The PET substrate was fed between the two electrodes (i.e., the corona electrode and the grounded electrode) at the various feeding speeds. The corona energy densities (E_{cor}) were controlled to be increased from 149 to 5263 kJ/m² by decreasing the PET feeding speed from 17 to 0.5 m/min.

The surface images and roughness of PET substrates were measured by atomic force microscope (AFM) as shown in **Figures 5(a), (b), and (c)** for nontreated, 4-times single-directionally corona treated, and [2 + 2]-times bidirectionally corona treated, respectively. The

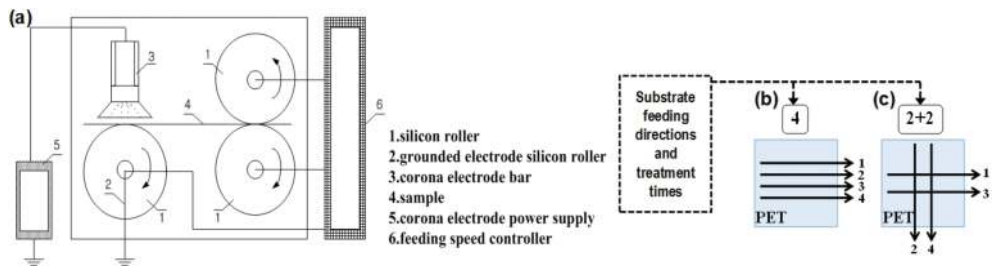


Figure 4. (a) The schematic diagram of the corona discharge system used in this study. The corona treatment methods such as (b) 4-times single-directionally corona treated and (c) [2 + 2]-times bidirectionally corona treated.

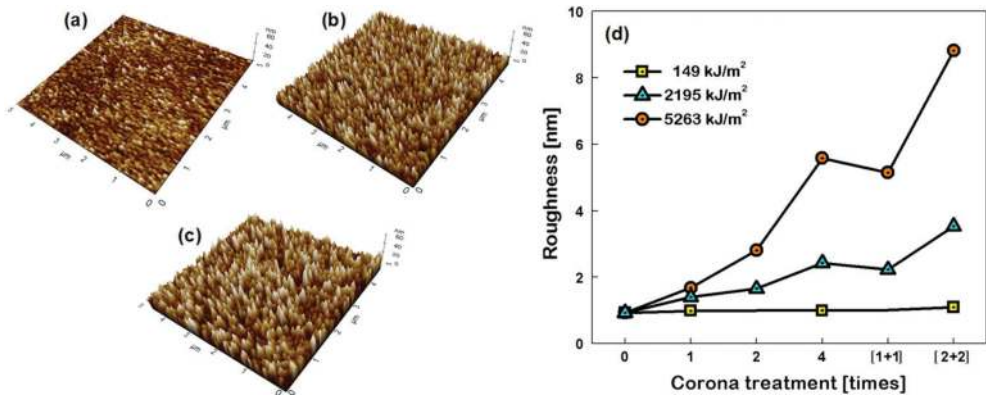


Figure 5. The AFM measurement data such as surface images and roughness for the various PET substrates: (a) nontreated, (b) 4-times corona treated, and (c) [2 + 2]-times corona treated. (d) The surface roughness indicated for three different corona energy densities in terms of feeding directions and the numbers of treatment.

root-mean-square surface roughness (σ_{rms}) was estimated, which is plotted in **Figure 5(d)**, in terms of the substrate feeding directions and the numbers of corona treatment. When the surface modification was performed at the low E_{cor} (149 kJ/m²), the change in σ_{rms} of the PET substrates appeared to have been negligibly small, regardless of the treatment manner. In contrast, when the PET substrates were treated at the higher E_{cor} (2195 or 5263 kJ/m²), the σ_{rms} values significantly increased as the treatment number increased. Also, the degree of the increase in σ_{rms} value due to the corona treatment was seen to have been bigger in the cases of the bidirectional treatment than in the cases of the single-directional treatment. For instance, the PET substrate that was bidirectionally [2 + 2]-times treated showed the σ_{rms} value of approximately 8.82 nm, whereas the PET substrate that was single-directionally treated 4-times yielded the σ_{rms} value of approximately 5.58 nm. This indicates that the bidirectionally treated method can effectively increase the surface area.

The contact angles (θ_c) of the PET substrates were measured from liquid drop images and compared in **Figure 6**, according to feeding directions and the numbers of treatment. In the θ_c measurement, two kinds of liquids were used such as water as a polar liquid (**Figure 6(a)–(d)**) and diiodomethane as a nonpolar or dispersive liquid (**Figure 6(e)–(h)**). As the number of corona treatment increased, the θ_c values based on water monotonically decreased, but the θ_c values based on diiodomethane continuously increased.

From the estimated θ_c results, the surface energies of the PET substrates were also calculated using the formula in the Owens-Wendt model [24]. **Figure 6(i)** shows the polar components (E_p) calculated from the water-based θ_c values, the dispersive components (E_D) obtained from the diiodomethane-based θ_c values, and the total surface energy (E_s) obtained from the sum of the E_p and E_D . The E_s value was observed to have increased as the number of the corona treatment increased in the single-direction (i.e., once and 4-times corona treated). Also, the higher E_s value was observed for the PET substrate that was [2 + 2]-times treated, compared with the PET substrate that was 4-times treated. These results indicate that the changes in the

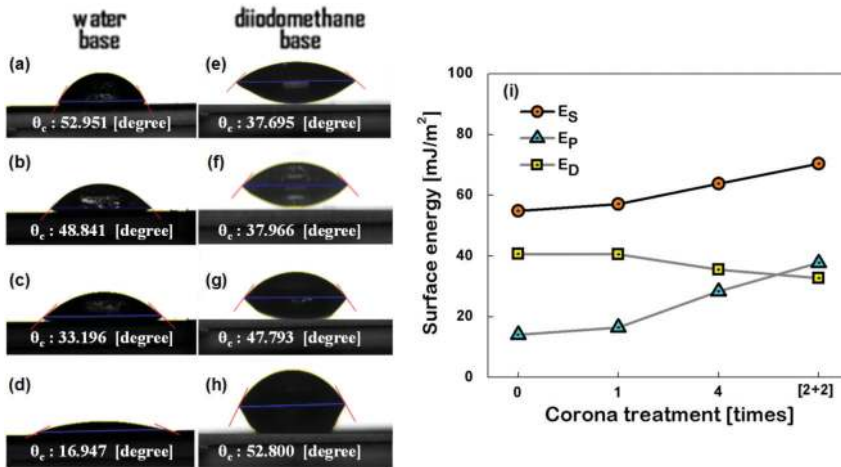


Figure 6. [(a)–(h)] The liquid drop images pictured from the PET substrates: (a) and (e) for nontreated, (b) and (f) for once corona treated, (c) and (g) for 4-times corona treated, (d) and (h) for [2 + 2]-times corona treated, and (i) the estimated E_S along with E_P and E_D components in terms of the PET feeding directions and the numbers of treatment.

E_S values of the PET substrates due to the corona treatment may cause the change of surface chemistries. Also, the results may confirm that the E_S of the PET substrates is closely related to the surface roughness.

It is known that the electrons, ions, and activated neutrons and protons produced from corona discharge react with the oxygen in the air to produce functional groups that contain oxygen, such as the COH and C=O groups, on the PET substrate surface [25]. The X-ray photoelectron spectroscopy (XPS) spectra of the carbon (C) 1s-state were measured for both nontreated and corona-treated PET substrates to investigate the changes in the surface chemistries of the PET substrates due to the corona treatment. For the nontreated PET substrate, three distinguishable peaks were observed and assigned to the aromatic hydrocarbons (284.7 eV), aliphatic esters (CH_2O , 286.3 eV), and carboxyl component (C-O-C=O , 288.7 eV) [26], as shown in **Figure 7**. In contrast, additional oxygen polar groups [27], such as phenolic-OH (286.5 eV), C=O (287.5 eV), and carboxyl acid (COOH, 289.2 eV), were observed for the corona-treated PET substrates. The relative contributions of each chemical group in the XPS spectra are summarized in **Table 1**, according to the corona treatment conditions. The relative contents of the oxygen polar groups increased by increasing the number of repetitions of the corona treatment and were larger especially for the bidirectionally corona-treated PET substrates.

It was also discovered that the PET's surface chemistry was changed from a hydrophobic nature to a hydrophilic nature after the corona treatment. It has been known that CNTs refined using acids such as HNO_3 may possess oxygen-related functional groups (e.g., carboxyl groups) on their outer walls [28], and also on the corona-treated PET substrate via a hydrogen bond [29]. This indicates that the adhesive force between the PET substrate and the CNTs can be enhanced by corona treatment of the PET substrate.

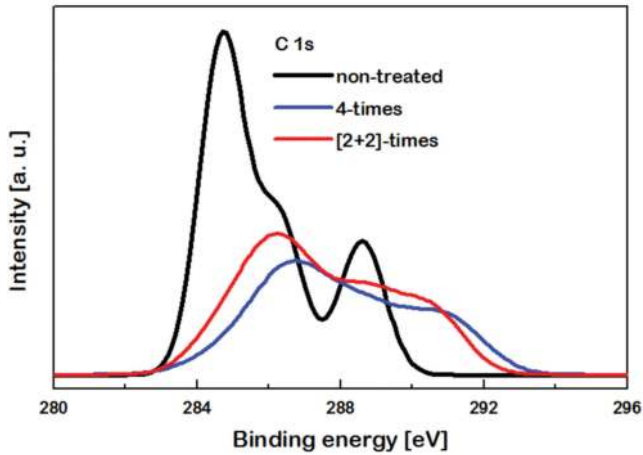


Figure 7. The XPS spectra for carbon (C 1s-state) measured for the nontreated and corona-treated PET substrates.

Assignment	Binding energy (eV)	Content (%)		
		Nontreated	Corona treated	
			4-times	[2 + 2]-times
Aromatic C–C	284.70	53.98	12.31	7.72
CH ₂ O	285.82–286.68	24.65	18.53	18.71
Phenolic-OH	288.34–288.93	21.37	19.59	18.11
C=O	286.50	—	11.23	10.64
C–O–C=O	287.51–287.67	—	20.11	22.10
COOH	288.88–289.03	—	18.23	22.72

Table 1. The binding energies and relative contents of the chemical bonds observed in the XPS spectra for the nontreated and corona-treated PET substrates.

3.2. The effect of corona treatment on the flexibility of CNT-TCEs

The effect of corona treatment of PET substrates on the flexibility CNT-TCEs has been investigated by measuring the changes in the CNTs' sheet resistance (R_{\square}) due to repetitive bending. Two bending tests such as outer bending and inner bending were carried out with a bending radius of 12 mm and a bending speed of 40 mm/s at an ambient temperature and pressure, as displayed in the insets of Figure 8(a) and (b), respectively. For all of the PET substrates that were nontreated or corona treated, the average R_{\square} value of the CNTs was observed to have been approximately $350 \pm 10 \Omega/\square$ before the bending test was conducted. As shown in Figure 8(a), the R_{\square} value of the CNTs deposited on the nontreated PET substrate significantly increased as the bending times increased, such that the R_{\square} value after

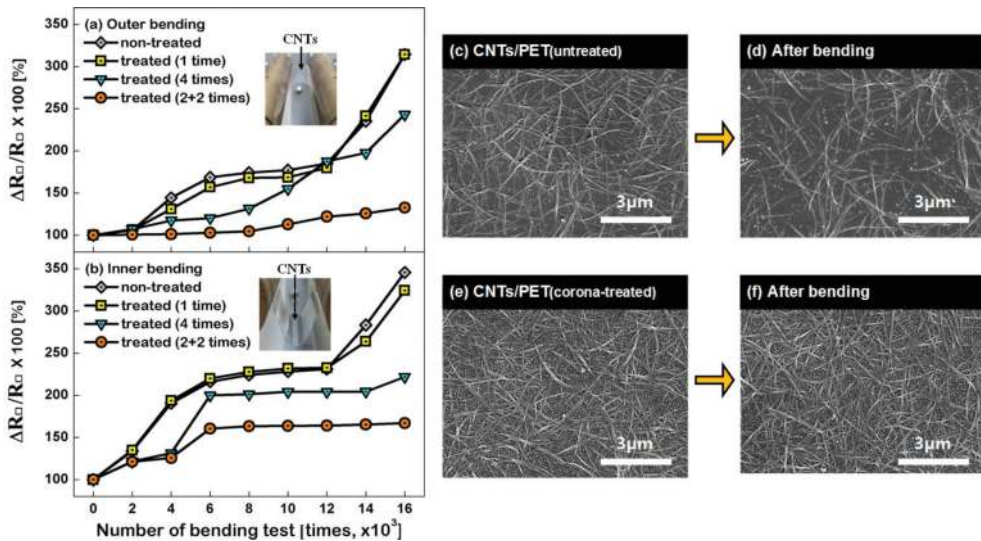


Figure 8. The changes in R_{\square} of CNTs during bending: (a) for outer bending and (b) for inner bending. [(c)–(f)] The comparison of FE-SEM images for the CNTs before and after bending. The photos (c) and (d) indicate the CNTs deposited on the nontreated PET substrates. The photos (e) and (f) indicate the CNTs deposited on the [2+2]-times corona-treated PET substrates.

16,000 times bending was almost more than 300% larger than the initial R_{\square} value before the bending. The increase in the CNTs' R_{\square} value due to bending may be attributed to the weak adhesion between the CNTs and the PET substrate. In contrast, the increase in the R_{\square} due to bending was observed to have been substantially alleviated for the CNTs that were deposited on the corona-treated PET substrates. As shown in **Figure 8(b)**, the similar results were observed in the case of the inner bending test. For both bending tests, the increase in R_{\square} after 16,000 bending repetitions was observed to have been minimal when the CNTs were deposited on the PET substrates that were [2 + 2]-times corona treated. Accordingly, the results shown in **Figure 8** confirm that the corona pretreatment improved the adhesion of the CNTs to the PET substrate.

Figure 8(c) and **(e)** shows the FE-SEM surface morphologies of the CNTs before they were bent, and **Figure 8(d)** and **(f)** displays the surface morphologies of the CNTs after they underwent bending. As shown in **Figure 8(d)**, the repetitive bending caused the marked reduction in the CNTs' density for the CNTs deposited on the untreated PET substrate. In contrast, as shown in **Figure 8(f)**, the CNTs deposited on the [2 + 2]-times corona-treated PET substrate revealed insignificant changes in the surface morphology even after the bending of 16,000 times. As a result, the higher surface roughness, the greater contact angles, and the higher surface energies, which the corona-treated PET substrates revealed, indicated that the surfaces of the PET substrates became hydrophilic from hydrophobic and thereby led to the improvement of adhesion between the CNTs and the PET substrates.

4. CNT-TCEs coated with PEDOT:PSS

Of the aforementioned in Section 1, CNTs have potential advantages such as chemical stability, thermal and electrical conductivity, mechanical strength, flexibility, solution processability, and low cost production. CNTs, however, still do not satisfy the electrical characteristics required for TCEs due to the uniform coating caused by their tubular structure and the large contact resistance at their tube-tube junction. To improve the electrical characteristics of CNTs, it was recently reported [30] that hybrid-type electrodes were introduced by combining CNTs with polymers via solution processes such as spray coating and spin coating. Adding the conductive polymers to the CNTs led to the decrease in the sheet resistance of CNTs; however, the electrical properties of the hybrid-type electrodes were sensitive to the deposition methods and combination conditions used to produce the electrodes. Furthermore, for the application of some devices such as display and TSPs, a neutral color of electrodes is required to prevent the distortion of the image color. However, the conductive polymer material is generally known to be tinged with the color blue, which may cause the problem that patterns of electrodes are revealed. Therefore, there is a necessity of studying how the chromaticity characteristic of CNTs changes or can be effectively adjusted according to the mixture with other materials (e.g., conductive polymers) for producing the hybrid-type electrodes.

In this section, hybrid-type transparent electrodes with characteristics desirable for flexible TCEs are introduced by coating CNTs with PEDOT:PSS via various methods such as spin coating, electrophoretic deposition (EPD), and electropolymerization. Their surface morphologies, sheet resistances, visible transmittances, and color properties have been characterized as functions of their preparation conditions. Also, to identify the flexible capabilities of the PEDOT:PSS-coated hybrid-type CNT-TCEs, the changes in their sheet resistances due to repetitive bending (up to 30,000 times) have been measured and compared with the results measured from the CNT-TCEs.

4.1. PEDOT:PSS coating via spin coating

For manufacturing hybrid-type CNT-TCEs, the CNTs were deposited on the PET substrates via spray coating by varying the spraying time from 10 to 80 s. Then, PEDOT:PSS layers were deposited on the CNTs via spin coating (for 1 min) by changing the spin speed within the range of 200–1500 rpm. The PEDOT:PSS-coated CNTs were dried in the oven for 5 min at 100°C and atmospheric pressure. The hybrid-type CNT-TCEs with various thickness combinations of CNTs and PEDOT:PSS layers were manufactured by controlling the spray time (for CNTs) and the spin speed (for PEDOT:PSS).

Figure 9(a) and **(c)** displays the electrical sheet resistances (R_{\square}) and visible range transmittances (T_{vis}) for CNTs (C_x) according to the increased spray time from 20 (C_1) to 80 s (C_7) and for PEDOT:PSS films (P_y) according to the decreased spin speed from 1500 (P_1) to 200 rpm (P_7), respectively. For the CNTs, both R_{\square} and T_{vis} monotonically decreased (e.g., R_{\square} from 3035 to 379 Ω/\square and T_{vis} from 93.2 to 80.4%) as the spray time increased. Therefore, there is a trade-off between R_{\square} and T_{vis} . For the PEDOT:PSS films, the similar trends in R_{\square} and T_{vis} appeared

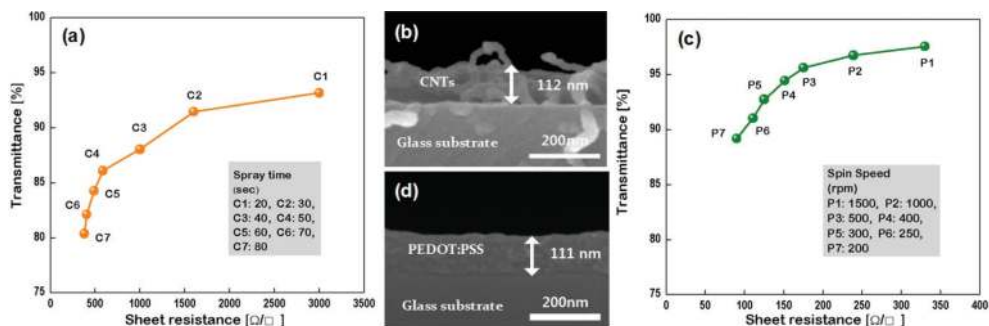


Figure 9. The sheet resistance and transmittance measured from the (a) CNTs and (c) PEDOT:PSS according to deposition thickness. The FE-SEM images (b) and (d) indicate the cross-sectional morphology of the CNTs specimen of C_7 and PEDOT:PSS specimen of P_7 .

(e.g., R_{\square} from 330 to 90 Ω/\square and T_{vis} from 97.5 to 89.2%) as the spin speed decreased. Also, the FE-SEM cross-sectional morphology of the CNTs and PEDOT:PSS electrodes are displayed in the inset of **Figure 9(b)** and **(d)**. The thickness of CNTs increased from 40.5 to 112 nm by increasing the spraying time from 20 to 80 s and the thickness of PEDOT:PSS films increased from 28.4 to 111 nm by decreasing the spinning speed from 1500 to 200 rpm. Accordingly, the decrease of T_{vis} as shown in **Figure 9(a)** and **(c)** was attributed to the increase in the thicknesses of CNTs and PEDOT:PSS layers.

For the hybrid electrodes (S_2), the R_{\square} and T_{vis} were also measured and the results are shown in **Figure 10(a)**. Here, the hybrid electrodes were fabricated by depositing the CNTs via spray coating under the same condition as the specimen C_3 and coating them with PEDOT:PSS by decreasing the spinning speed from 1500 (S_1) to 200 rpm (S_3) via spin coating. For the hybrid-type specimens (S_2), both R_{\square} and T_{vis} decreased (e.g., R_{\square} from 298 to 73.49 Ω/\square and T_{vis} from 87.52 to 78.84%) as the spinning speed decreased because the thickness of the PEDOT:PSS films increased from 28.4 to 114.9 nm with a decrease in the spinning speed from 1500 to 200 rpm. It was observed that the decrease in the T_{vis} due to the coating of the PEDOT:PSS films was trivial, while the R_{\square} of CNTs was substantially reduced by the coating of PEDOT:PSS. For instance, the hybrid electrode of S_1 , which was fabricated by coating the CNTs (C_3) with the PEDOT:PSS film at the spinning speed of 1500 rpm, had an R_{\square} of approximately 298 Ω/\square and a T_{vis} of 87.52%, whereas the CNTs (C_3) showed a much higher R_{\square} (959.3 Ω/\square) and a slightly higher T_{vis} (88.80%). This was because the PEDOT:PSS particles filled up the voids between the tubes in the CNTs as shown in **Figure 10(e)** and thereby formed a conduction bridge for electron transfer, inducing a decrease in the tube-tube junction resistance and the percolation threshold, eventually enhancing the conductivity of the hybrid electrodes [31].

In addition to low electric sheet resistance and high transmittance, TCEs should also satisfy the chromatic characteristics approaching no color. Generally, the chromaticity of a TCE can be determined by using the three-dimensional color space (namely, L^* , a^* , and b^*) where each coordinate axis expresses specific color components [32], as shown in **Figure 11(a)**. Here, L^* means brightness having the numerical value between 0 (lowest) and 100 (highest). The a^*

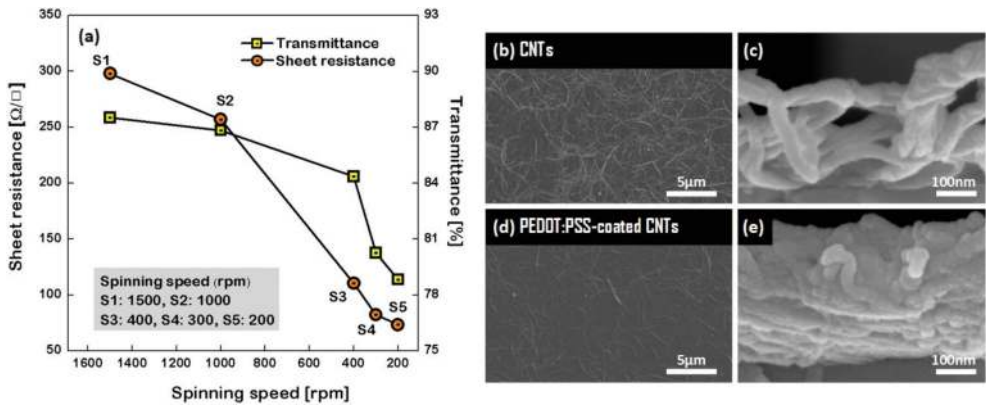


Figure 10. (a) The sheet resistance and average transmittance measured from the PEDOT:PSS-coated CNTs hybrid electrodes as a function of the spinning speed used to coat the PEDOT:PSS films via spin coating. The FE-SEM surface and cross-sectional images: (b) and (c) for CNTs, (d) and (e) for PEDOT:PSS-coated CNTs.

(redness) value is the positive definiteness (+) that is close to the color red as it increases and it is close to the color green as it increases with the negative definiteness (-). Also, the b^* (yellowness) value is close to yellow color as it increases with the positive definiteness and it appears to be blue color as it increases with the negative definiteness.

Figure 11(b)–(d) shows the measured results of chromaticity characteristics for three kinds of TCEs such as (b) CNTs, (c) PEDOT:PSS, and (d) PEDOT:PSS-coated CNTs. For the CNTs, the b^* gradually increased in the negative direction of sign from about 0.58 to 1.58 as the spraying time increased, whereas the a^* showed neighboring zero regardless of the spraying time. For the PEDOT:PSS films, both a^* and b^* monotonically increased in the negative direction of

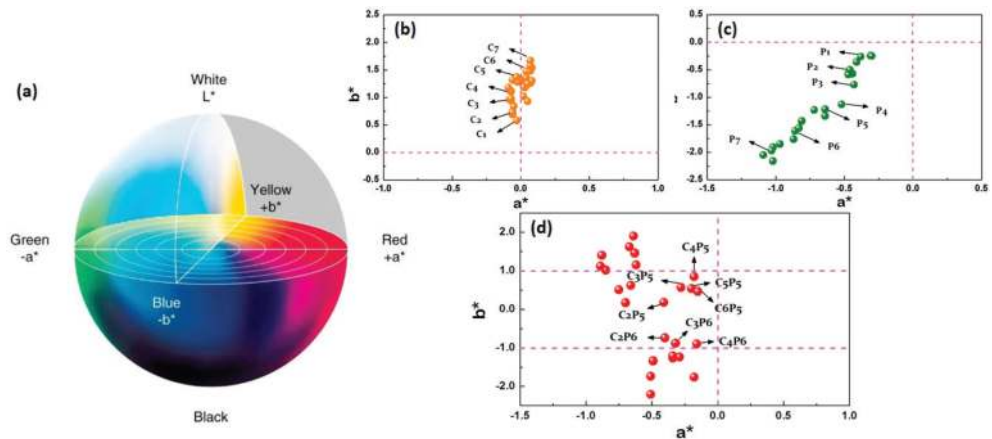


Figure 11. (a) Color space (L^* , a^* , and b^*). [(b)–(d)] The measured chromatic parameters (a^* and b^*) for various electrodes: (b) for CNTs (C_x), (c) for PEDOT:PSS (P_x), and (d) for PEDOT:PSS-coated CNTs (C_xP_x).

sign as the spinning speed decreased (e.g., the a^* from -0.31 to -1.09 and the b^* from -0.24 to -2.05). Namely, increasing the thicknesses of CNTs and PEDOT:PSS layers led to the decrease in their sheet resistances, but it resulted in the deterioration of their chromaticity characteristics, especially for the yellowness. Here, it should be noted that the b^* values of the CNTs and PEDOT:PSS layers changed in the mutually opposite directions of sign according to the thicknesses of CNTs and PEDOT:PSS layers. **Figure 11(d)** displays the measured results of characteristic values of a^* and b^* of the PEDOT:PSS-coated CNTs manufactured by variously combining the deposition conditions of CNTs (i.e., the spraying times) and the coating conditions of PEDOT:PSS (i.e., the spinning speeds). For the C_3P_5 specimen, the a^* value of -0.28 was located between those of CNTs and PEDOT:PSS (i.e., -0.08 for C_3 and -0.64 for P_5) and the b^* value of 0.57 was also between those of CNTs and PEDOT:PSS (i.e., 0.96 for C_3 and -1.22 for P_5). This indicates that hybrid-type electrodes with CNTs and PEDOT:PSS combined can possess the better color properties compared with those of single electrodes (e.g., CNTs or PEDOT:PSS) due to their complementary color relation.

4.2. PEDOT:PSS coating via electrophoretic deposition (EPD)

The coating of CNTs with PEDOT:PSS films via EPD was performed using a mixed solution of PEDOT:PSS (5 ml) and isopropyl alcohol (IPA, 100 ml). In the EPD process, the PEDOT:PSS films were deposited on the anode electrode where the spacing between the anode (i.e., CNTs) and the cathode (i.e., Cu) was kept at 10 mm and the DC bias voltage of 100 V was applied during the changing of the process time within the range of 20–40 s.

For the hybrid electrodes (E_j) which were fabricated by coating the CNTs (C_3) with the PEDOT:PSS films via the EPD method, the R_{\square} and T_{vis} were measured. The results are shown in **Figure 12(a)**, according to the increase in the EPD time from 20 (E_1) to 40 s (E_5). **Figure 12(a)** shows the relationships between the R_{\square} and T_{vis} measured from the two different hybrid electrodes such as the S_z specimens fabricated by coating the CNTs (C_3) with the PEDOT:PSS films

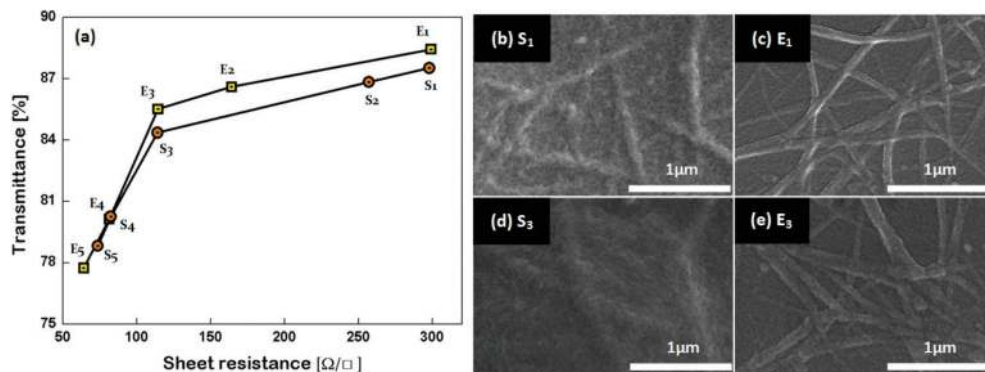


Figure 12. (a) The sheet resistances and average transmittances of the hybrid electrodes, where the PEDOT:PSS films were coated on the CNTs via spin coating (i.e., the specimens denoted as S_j) or EPD (i.e., the specimens denoted as E_j), along with the FE-SEM images of the S_1 and E_1 specimens. [(b)–(e)] The surface morphologies of the specimens (b) S_1 , (c) E_1 , (d) S_3 , and (e) E_3 .

via spin coating and the E_z specimens fabricated by coating the CNTs (C_3) with the PEDOT:PSS films via EPD. For the hybrid electrodes E_z (i.e., using EPD), the changes in the R_{\square} and T_{vis} were observed to have been similar to those of the hybrid electrodes S_z (i.e., using spin coating). Here, it may be noted that the T_{vis} of the hybrid electrode E_3 was measured as 85.52%, slightly higher than that (84.36%) of the hybrid electrode S_3 , whereas both hybrid electrodes had almost the same R_{\square} values such as approximately $114.4 \Omega/\square$ for E_3 and $110.5 \Omega/\square$ for S_3 . The similar trend was also observed for the hybrid electrodes of S_1 and E_1 .

Generally, the film deposition via EPD is generally achieved by the motion of the charged particles that are dispersed in a suitable solvent toward an electrode under an applied electric field [33]. Accordingly, the results of **Figure 12(a)** can be explained by comparing the surface morphologies of the hybrid electrodes, which are shown in **Figure 12(b)–(e)**. It was observed from the surface images of **Figure 12(b)** and **(d)** (i.e., the hybrid electrodes of S_1 and S_3) that the PEDOT:PSS layer was deposited not only on the region where the CNTs existed but also on the region where no CNTs existed. On the other hand, the surface images of **Figure 12(c)** and **(e)** (i.e., the hybrid electrodes of E_1 and E_3) showed that most of the PEDOT:PSS layer covered the area near the CNTs. Therefore, the observation that the sample E_1 (or E_3) displayed the higher transmittance as compared to the sample S_1 (or S_3) was because there were regions where the PEDOT:PSS films were hardly coated.

To compare the flexibility of the CNTs and the hybrid electrodes (i.e., PEDOT:PSS-coated CNTs either using EPD (E_z) or spin coating (S_z)), the bending tests were analyzed, and the results are shown in **Figure 13(a)** as functions of the number of bending tests (up to 30,000). In the case of the CNTs, the R_{\square} increased continuously as the number of bending times increased and appeared to almost have doubled after the completion of the bending test. On the contrary, the increase in the R_{\square} was mitigated for the hybrid electrodes, indicating an improvement in flexibility. The flexibility-enhancement effect was higher by increasing the thickness of the coated PEDOT:PSS layer (i.e., from S_1 to S_3 or from E_1 to E_3). This may be because the PEDOT:PSS film induced the physical gripping of the CNTs to enable them to adhere better to the underlying PET substrate [34]. This may also be due to the chemical bonds between the PEDOT:PSS film and the corona-treated PET substrate or between the PEDOT:PSS film and the acid-treated CNTs [35].

Figure 13(b)–(g) shows the changes of FE-SEM surface morphologies due to bending, measured from the electrodes of CNTs (C_3) and hybrids (S_3 and E_3). **Figure 13(b)**, **(c)**, and **(d)** indicates their images measured before bending and **Figure 13(e)**, **(f)**, and **(g)** shows images measured after bending of 30,000 times. For the C_3 electrode (CNTs), the density of the CNTs was significantly decreased from about 1.97 to 1.52 tubes/ μm^2 after bending. On the contrary, the density of the CNTs in the S_3 and E_3 electrodes (hybrid) hardly changed after bending. This may confirm that the hybrid electrodes have more potential in flexibility as compared to the CNTs. In addition, the hybrid electrode fabricated via spin coating showed less change in resistance than the hybrid electrode fabricated via EPD. The deposition of PEDOT:PSS occurs mainly on the surface of the CNTs in EPD, whereas in spin coating, the deposition of PEDOT:PSS occurs not only on the CNTs' surface but also on the PET substrate where no CNTs exist. In the case of the EPD-produced hybrid electrodes, accordingly, if the CNTs are

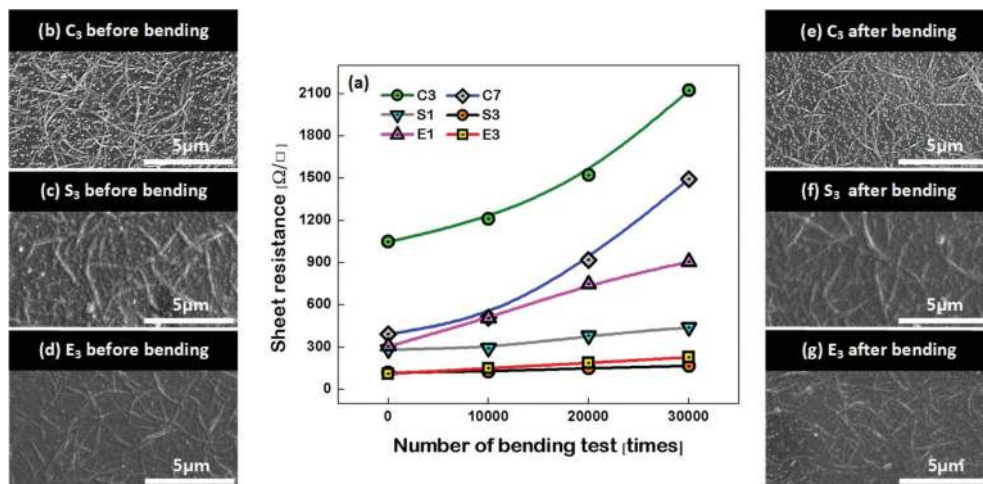


Figure 13. (a) The changes in the sheet resistances due to bending tests (up to 30,000 times), measured from the various electrodes such as CNTs (i.e., C₃ and C₇) and PEDOT:PSS-coated CNTs (i.e., S₁, S₃, E₁, and E₃). [(b)–(g)] The changes of FE-SEM surface morphologies due to bending, measured from the electrodes of CNTs (C₃) and hybrids (S₃ and E₃). Here, (b), (c), and (d) indicate their images obtained before bending (left photos), and (e), (f), and (g) obtained after bending (right photos) of 30,000 times.

detached during the bending test, then the PEDOT:PSS layer on the CNTs is also detached and thus, the resistance of the electrodes will inevitably increase. In contrast, in the case of the hybrid electrodes fabricated via spin coating, the increase in resistance may be insignificant even if they experience the detachment of CNTs due to bending because the conductive PEDOT:PSS layers still remain.

5. Effects of CNT-coating and washing on properties of copper meshes

Metal meshes have been developed as the alternative transparent electrodes to replace the conventional ITO due to their low electric sheet resistance and high visible transmittance. However, metal meshes have a relatively high reflectance generated by metals, and several metals, such as gold (Au) and copper (Cu), are generally tinged with specific colors, leading to a visibility problem. The most commonly used materials for the metal-based TCEs are silver (Ag) and Cu. Compared with Ag, Cu is more abundant and less expensive, but it has higher resistivity. Also, Cu is generally tinged with a red-orange color [36], requiring it to be coated with black materials capable of absorbing light effectively. CNTs are known as excellent absorbers of visible light [37] and have advantages in terms of chemical stability, thermal and electric conductivity, mechanical strength, and flexibility. To improve the visibility of metal mesh electrodes, the authors recently introduced hybrid-type TCEs fabricated via the combination of metal meshes with CNTs [38].

Cu films were deposited on glass substrates (Corning, Eagle 2000, $3 \times 3 \text{ cm}^2$) at room temperature via RF sputtering at 80 W power and 30 mTorr working pressure. Cu meshes were formed via lithography to produce a $200 \mu\text{m}$ line spacing and a $10 \mu\text{m}$ line width. Single-walled CNT powder (NanoAmor 1284Y), 15 mg) was placed in a mixture of H_2SO_4 (20 ml) and HNO_3 (10 ml) at a 2:1 volume ratio and was ultrasonicated for 30 min to eliminate the impurities such as the metal catalysts and amorphous carbons. The CNT solution was dispersed for 15 min using an ultrasonic generator after adding a dispersant of magnesium nitrate ($\text{Mg}(\text{NO}_3)_2 \cdot 6\text{H}_2\text{O}$, 15 mg) and isopropyl alcohol (IPA, 100 ml). CNTs were deposited on the Cu meshes via the EPD process, conditions of which were previously reported in the authors' recent paper. The thickness of the CNTs was controlled by varying the EPD time from 5 to 15 s. Finally, for post-washing, the CNT-coated Cu meshes were dipped in deionized water by varying the post-washing time from 0 to 30 s.

Figure 14(a) and (b) displays the FE-SEM photos of the fabricated Cu mesh and the CNT-coated Cu mesh along with the enlarged photo of the surface morphology of the CNT coating layer, respectively. It can be clearly seen that CNTs were used to selectively coat only the surfaces where the Cu mesh patterns had been formed. The thickness profiles of the CNT-coated Cu meshes measured before and after post-washing are shown in the inset of Figure 14(c). The thickness of the Cu mesh was approximately 106 nm, and it was increased to approximately 913 nm after the Cu mesh was coated with CNTs via the 15 s EPD process. Meanwhile, the thickness of the CNT-coated Cu mesh was considerably decreased as the post-washing process progressed, and it was approximately 237 nm after 30 s post-washing, as shown in Figure 14(c). This was because some of the CNTs were detached from the Cu mesh during the washing process. All of the Cu mesh specimens considered in this study are summarized in Table 2.

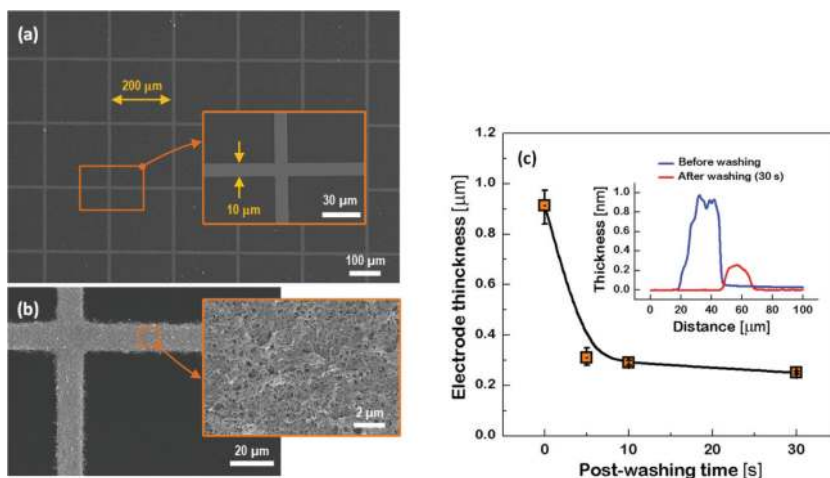


Figure 14. [(a) and (b)] The FE-SEM photos for a pristine Cu mesh with a $200 \mu\text{m}$ line spacing and a $10 \mu\text{m}$ line width and a CNT-coated Cu mesh including the surface morphology of the CNT coating layer. (c) The change in the thickness of the CNT-coated Cu mesh as a function of the post-washing time and the thickness profiles (inset) of the CNT-coated Cu meshes measured before and after post-washing (30 s).

Sample	EPD time (min)	Washing time (s)	Thickness of CNTs (nm)	T_{vis} (%)	R_{vis} (%)	a^*	b^*
Cu(p)	—	—	106.3	90.71	11.83	1.91	1.92
CCu-1	5	—	323.6	90.24	8.91	1.54	1.88
CCu-2	10	—	546.2	89.80	8.44	1.15	1.61
CCu-3	15	—	807.0	89.79	7.89	0.88	1.13
W-CCu-1	5	30	95.6	90.18	8.51	1.44	1.51
W-CCu-2	10	30	110.9	89.98	7.79	0.96	0.58
W-CCu-3	15	30	130.7	89.83	7.37	0.16	-0.55

Table 2. The sample ID's considered in this study, along with their preparation conditions and the summary of measured quantities.

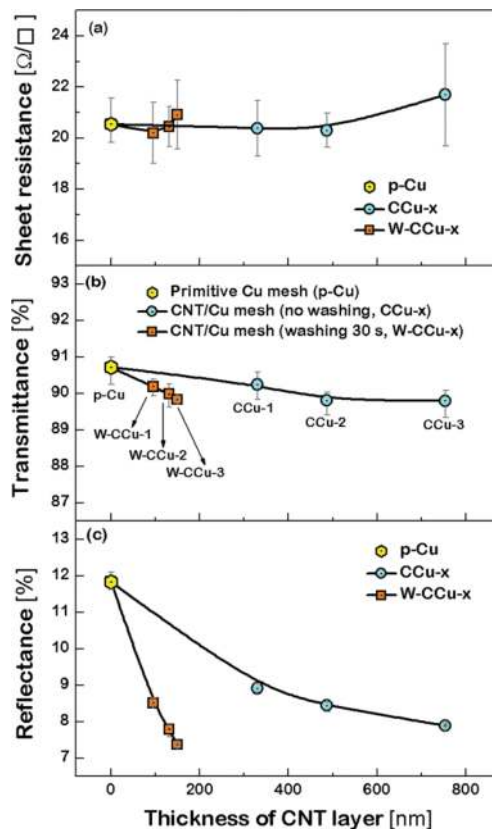


Figure 15. (Left) The results of: (a) sheet resistance, (b) transmittance, and (c) reflectance, measured from pristine Cu mesh (denoted by “p-Cu”), and CNT-coated Cu-meshes before washing and after 30 s post-washing (denoted by “CCu-x” and “W-CCu-x” (“x” = 1, 2, and 3), respectively), in terms of the CNT's thicknesses.

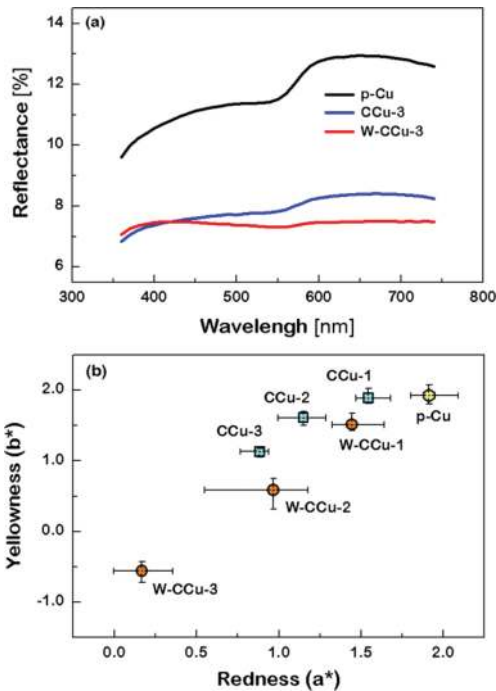


Figure 16. (Right) (a) The reflectance spectra of primitive Cu-mesh (p-Cu), and CNT-coated Cu meshes before washing (CCu-3) and after washing (W-CCu-3). (b) The estimated chromatic parameters of redness (a^*) and yellowness (b^*) for all the specimens fabricated in this study.

Figure 15(a)–(c) shows the results of the sheet resistance, transmittance, and reflectance measured from the pristine Cu mesh and the CNT-coated Cu meshes before and after post-washing, in terms of the CNT's thicknesses. The sheet resistance and transmittance of the Cu meshes were hardly affected by the CNT coating and the CNT's thickness, and was also marginally changed by post-washing. For all of the specimens, their sheet resistance and transmittance values were in the range of 20.2–21.5 Ω/\square and 89.8–90.7%, respectively. On the other hand, the reflectance of the Cu mesh was significantly reduced by the CNT coating. This indicated that the CNT coating layer played the role of suppressing the visible light reflected from the Cu mesh. In **Figure 15(c)**, it is noted that the reflectance of the CNT-coated Cu mesh was further reduced after it underwent post-washing (e.g., 7.89% for C-Cu-3 and 7.37% for W-CCu-3, respectively).

Generally, the color property of a metal mesh is closely related to its reflectance spectrum, from which the chromatic parameters, redness (a^*) and yellowness (b^*), can be determined. Both the a^* and b^* components being closer to zero indicate that the metal mesh appears nearly colorless. **Figure 16(a)** shows the reflectance spectra measured from the p-Cu, CCu-3, and W-CCu-3 specimens, and **Figure 16(b)** shows the redness and yellowness values estimated from all of the specimens. The pristine Cu mesh revealed a stair-like spectrum where the level of reflectance was demarcated at a wavelength of around 560 nm, and its redness

and yellowness values were approximately 1.91 and 1.92, respectively. This may be the cause of the red-orange tint of the pristine Cu mesh. In contrast, such disparity in reflectance nearly disappeared when the Cu meshes were coated with CNTs, and the flat-type spectra with much lower reflectance levels were observed for the CNT-coated Cu meshes. Both a^* and b^* values considerably decreased as the CNT's thickness was increased, and further decreased when the CNT-coated Cu meshes underwent post-washing. For instance, the a^* and b^* values of the CCu-3 mesh were approximately 0.88 and 1.13, respectively, and those of the W-CCu-3 mesh were approximately 0.16 and -0.55 , respectively.

In order to discover why the CNT-coated Cu meshes exhibited such lower reflectance and smaller a^* and b^* after they underwent post-washing, the changes in their atomic components and surface chemistry were investigated. **Figure 17(a)** and **(b)** shows the Auger electron spectroscopy (AES) measurement results, which indicate the relative atomic contents of C, O, Mg, and Cu for the CNT-coated Cu meshes before and after post-washing, respectively, as a function of the sputtering time (0–25 min) used for the AES analysis. For the CCu-3 specimen as shown in **Figure 17(a)**, the C atom content was always greater than the Cu atom content, while for the W-CCu-3 specimen as shown in **Figure 17(b)**, the Cu atom content exceeded the C atom content as the sputtering time was around 15 min, indicating that the layer was changed from a CNT region to a Cu mesh region. This was attributed to the decrease in the Cu mesh's thickness due to the detachment of the CNTs after post-washing. It was also observed that the CCu-3 specimen contained the Mg atoms with an atomic content higher than about 10%. This was because magnesium nitrate ($\text{Mg}(\text{NO}_3)_2 \cdot 6\text{H}_2\text{O}$) was

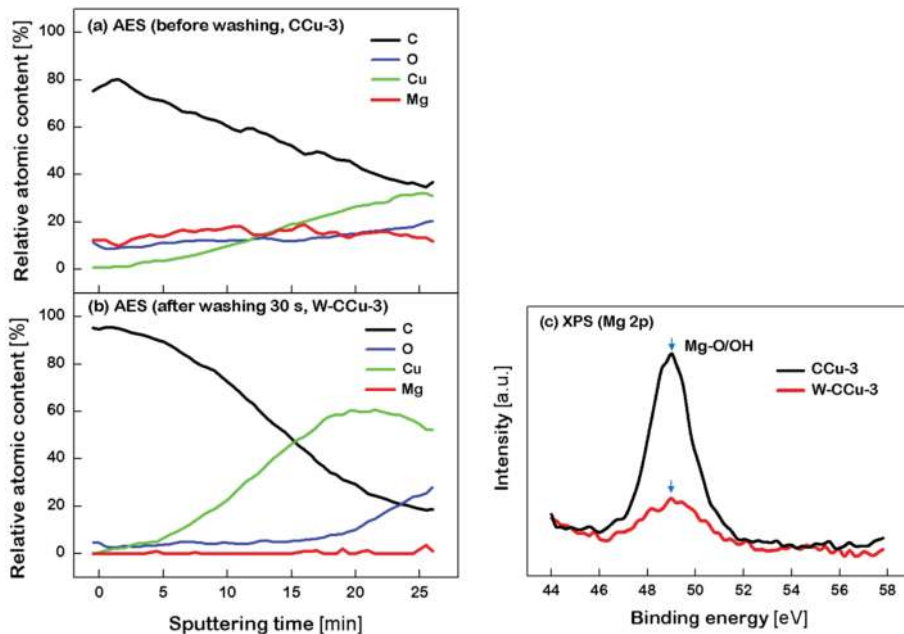


Figure 17. The relative atomic contents (measured by AES) of C, O, Mg, and Cu incorporated in the CNT-coated Cu mesh: (a) before washing (CCu-3) and (b) after washing (W-CCu-3). (c) The XPS Mg 2p spectra for CCu-3 and W-CCu-3 specimens.

used as the dispersant for the CNT suspension. On the other hand, it was discovered that the Mg content was almost negligible in the W-CCu-3 specimen, indicating that most of the Mg atoms were removed by post-washing. **Figure 17(c)** compares the XPS Mg 2p spectra of the CCu-3 and W-CCu-3 specimens. The XPS peak corresponding to Mg-O/OH [39] was observed at around 49 eV, and the peak intensity of the W-Cu-3 specimen was much smaller than that of the Cu-3 specimen, indicating that the Mg component was removed by post-washing. Accordingly, it was suggested that the lower reflectance and the smaller chromatic parameters, which were observed when the CNT-coated Cu meshes underwent post-washing, resulted from the removal of the residual Mg element.

6. Conclusion

CNTs have excellent chemical stability, thermal and electrical conductivity (high intrinsic conductivity), mechanical strength, flexibility, solution processability, and potential for production at a low cost. Based on these advantages, the CNT-based TCEs are presented. In Section 3, it was illustrated that the adhesion of the CNTs was remarkably improved after the surface modification via corona pretreatment of the PET substrates. Then, in Sections 4 and 5, the hybrid-type TCEs, which can be commercialized in various applications, were fabricated and their characteristics were demonstrated. In particular, the studies about improving the electrical conductivity and transmittance of CNTs-TCEs may warrant increased interest. Finally, in Section 5, the metal-based TCEs coated with CNTs were considered as an effective structure to resolve the high reflectance generated by the intrinsic properties of metals. Until now, the TCEs fabricated using only CNTs had insufficient properties for applications to electronic devices. Various hybrid-types of CNT-based TCEs, however, could have potential in the application to next-generation flexible and stretchable electronics to overcome various issues.

Author details

Bu-Jong Kim and Jin-Seok Park*

*Address all correspondence to: jinsp@hanyang.ac.kr

Department of Electronic Systems Engineering, Hanyang University, Ansan, Gyeonggi-do, Republic of Korea

References

- [1] Cann M, Large MJ, Henley SJ, Milne D, Sato T, Chan H, Jurewicz I, Dalton AB. High performance transparent multi-touch sensors based on silver nanowires. *Materials Today Communications*. 2016;7:42-50. DOI: 10.1016/j.mtcomm.2016.03.005

- [2] Lordan D, Burke M, Manning M, Martin A, Amann A, O'Connell D, Murphy R, Lyons C, Quinn AJ. Asymmetric pentagonal metal meshes for flexible transparent electrodes and heaters. *ACS Applied Materials & Interfaces*. 2017;**9**:4932-4940. DOI: 10.1021/acsami.6b12995
- [3] Parkb J-M, Wang Z-J, Kwon D-J, Ga-Young G, Lawrence DeVries K. Electrical properties of transparent CNT and ITO coatings on PET substrate including nano-structural aspects. *Solid-State Electronics*. 2013;**79**:147-151. DOI: 10.1016/j.sse.2012.05.037
- [4] Song C-H, Ok K-H, Lee C-J, Kim Y, Kwak M-G, Han CJ, Kim N, Byeong-Kwon J, Kim J-W. Intense-pulsed-light irradiation of Ag nanowire-based transparent electrodes for use in flexible organic light emitting diodes. *Organic Electronics*. 2015;**17**:208-215. DOI: 10.1016/j.orgel.2014.12.015
- [5] Highly conductive PEDOT:PSS transparent electrode prepared by a post-spin-rinsing method for efficient ITO-free polymer solar cells. *Solar Energy Materials & Solar Cells*. 2016;**144**:143-149. DOI: 10.1016/j.solmat.2015.08.039
- [6] Mallikarjuna K, Hwang H-J, Chunga W-H, Kim H-S. Photonic welding of ultra-long copper nanowire network for flexible transparent electrodes using white flash light sintering. *RSC Advances*. 2016;**6**:4770-4779. DOI: 10.1039/c5ra25548a
- [7] Hajimammadov R, Csendes Z, Ojakoski J-M, Lorite GS, Mohl M, Kordas K. Nonlinear electronic transport and enhanced catalytic behavior caused by native oxides on Cu nanowires. *Surface Science*. 2017;**663**:16-22. DOI: 10.1016/j.susc.2017.04.011
- [8] Jung S-G, Lee HJ, Hwang JH, Shim YS, Kim KN, Park CH, Park YW, Byeong Kwon J. Tungsten oxide buffer layer on silver nanowires for electrically stable, flexible, transparent hybrid electrodes using solution process. *Late-News Poster*. 2015;**46**(1):1386-1387. DOI: 10.1002/sdtp.10133
- [9] Park S, Vosguerichian M, Bao Z. A review of fabrication and applications of carbon nanotube film-based flexible electronics. *Nanoscale*. 2013;**5**:1727-1752. DOI: 10.1039/c3nr33560g
- [10] Akimitsu Narita, editor. *Bottom-Up Synthesis of Chemically Precise Graphene Nanoribbons*. Japan; 2013. 280 p
- [11] Ok K-H, Kim J, Park S-R, Kim Y, Lee C-J, Hong S-J, Kwak M-G, Kim N, Han CJ, Kim J-W. Ultra-thin and smooth transparent electrode for flexible and leakage-free organic light-emitting diodes. *Scientific reports*. 2015;**5**:9464. DOI: 10.1038/srep09464
- [12] Blackburn JL, Barnes TM, Beard MC, Kim Y-H, Tenent RC, McDonald TJ, Bobby T, Coutts TJ, Heben MJ. Transparent conductive single-walled carbon nanotube networks with precisely tunable ratios of semiconducting and metallic nanotubes. *ACS Nano*. 2008;**2**(6):1266-1274. DOI: 10.1021/nn800200d

- [13] Feng Y, Miyata Y, Matsuishi K, Kataura H. High-efficiency separation of single-wall carbon nanotubes by self-generated density gradient ultracentrifugation. *Journal of Physical Chemistry C*. 2011;**115**:1752-1756. DOI: 10.1021/jp1100329
- [14] Chandra B, Afzali A, Khare N, El-Ashry MM, Tulevski GS. Stable charge-transfer doping of transparent single-walled carbon nanotube films. *Chemistry of Materials*. 2010;**22**:5179-5183. DOI: 10.1021/cm101085p
- [15] Hou P-X, Liu C, Cheng H-M. Purification of carbon nanotubes. *Carbon*. 2008;**46**:2003-2025. DOI: 10.1016/j.carbon.2008.09.009
- [16] Park T-J, Banerjee S, Hemraj-Benny T, Wong SS. Purification strategies and purity visualization techniques for single-walled carbon nanotubes. *Journal of Materials Chemistry*. 2006;**16**:141-154. DOI: 10.1039/b510858f
- [17] Rastogi R, Kaushal R, Tripathi SK, Sharma AL, Kaur I, Bharadwaj LM. Comparative study of carbon nanotube dispersion using surfactants. *Journal of Colloid and Interface Science*. 2008;**328**:421-428. DOI: 10.1016/j.jcis.2008.09.015
- [18] Jang EY, Kang TJ, Im H, Baek SJ, Kim S, Jeong DH, Park YW, Kim YH. Macroscopic single-walled-carbon-nanotube fiber self-assembled by dip-coating method. *Advanced Materials*. 2009;**21**:4357-4361. DOI: 10.1002/adma.200900480
- [19] Chatzikomis C, Pattinson SW, Koziol KKK, Hutchings IM. Patterning of carbon nanotube structures by inkjet printing of catalyst. *Journal of Materials Science*. 2012;**47**:5760-5765. DOI: 10.1007/s10853-012-6467-2
- [20] Sung WY, Lee SM, Kim WJ, Ok JG, Ho YL, Kim YH. New approach to enhance adhesions between carbon nanotube emitters and substrate by the combination of electrophoresis and successive electroplating. *Diamond & Related Materials*. 2008;**17**:1003-1007. DOI: 10.1016/j.diamond.2008.03.001
- [21] Urbaniak-Domagala W. Pretreatment of polypropylene films for the creation of thin polymer layers, part 1: The use of chemical, electrochemical, and UV methods. *Journal of Applied Polymer Science*. 2011;**122**:2071-2080. DOI: 10.1002/app.34301
- [22] Liua X-D, Shenga D-K, Gaoa X-M, Tong-Bing L, Yang Y-M. UV-assisted surface modification of PET fiber for adhesion improvement. *Applied Surface Science*. 2013;**264**:61-69. DOI: 10.1016/j.apsusc.2012.09.107
- [23] Gorenšek M, Gorjanc M, Bukošek V, Kovac J, Jovancić P, Mihailović D. Functionalization of PET fabrics by corona and nano silver. *Textile Research Journal*. 2010;**80**(3):253-262. DOI: 10.1177/0040517509105275
- [24] Owens DK, Wendt RC. Estimation of the surface free energy of polymers. *Journal of Applied Polymer Science*. 1969;**13**:1741-1747. DOI: 10.1002/app.1969.070130815

- [25] Park S-J, Jin J-S. Effect of corona discharge treatment on the dyeability of low-density polyethylene film. *Journal of Colloid and Interface Science*. 2001;**236**:155-160. DOI: 10.1006/jcis.2000.7380
- [26] O'Hare L-A, Smith JA, Leadley SR, Parbhoo B, Goodwin AJ, Watts JF. Surface physico-chemistry of corona-discharge-treated poly(ethylene terephthalate) film. *Surface and Interface Analysis*. 2002;**33**:617-625. DOI: 10.1002/sia.1429
- [27] Jacobs T, Carbone E, Morent R, De Geyter N, Reniers F, Leys C. Surfacedmodification of polymer films with a remote atmospheric pressure d.C. glow discharge: Influence of substrate location. *Surface and Interface Analysis*. 2010;**42**:1316-1320. DOI: 10.1002/sia.3319
- [28] Jia H, Lian Y, Ishitsuka M, Nakahodo T, Yutaka M, Tsuchiya T, Wakahara T, Akasaka T. Centrifugal purification of chemically modified single-walled carbon nanotubes. *Science and Technology of Advanced Materials*. 2005;**6**:571-581. DOI: 10.1016/j.stam.2005.08.004
- [29] Sahoo NG, Cheng HKF, Bao H, Pan Y, Li L, Chan SH. Covalent functionalization of carbon nanotubes for ultimate interfacial adhesion to liquid crystalline polymer. *Soft Matter*. 2011;**7**:9505-9514. DOI: 10.1039/c1sm05360d
- [30] Zhang J, Gao L, Sun J, Liu Y, Wang Y, Wang J. Incorporation of single-walled carbon nanotubes with PEDOT/PSS in DMSO for the production of transparent conducting films. *Diamond & Related Materials*. 2012;**22**:82-87. DOI: 10.1016/j.diamond.2011.12.008
- [31] Xiao G, Ye T, Jianping L, Zhang Z. Highly conductive and transparent carbon nanotube composite thin films deposited on polyethylene terephthalate solution dipping. *Thin Solid Films*. 2010;**518**:2822-2824. DOI: 10.1016/j.tsf.2009.11.021
- [32] Hecht DS, Thomas D, Liangbing H, Ladous C, Lam T, Park Y, Irvin G, Drzaic P. Carbon-nanotube film on plastic as transparent electrode for resistive touch screens. *Journal of the SID*. 2009;**17**(11):941-946. DOI: 10.1889/JSID17.11.941
- [33] Boccaccini AR, Cho J, Roether JA, Thomas BJC, Jane Minay E, Shaffer MSP. Electrophoretic deposition of carbon nanotubes. *Carbon*. 2006;**44**:3149-3160. DOI: 10.1016/j.carbon.2006.06.021
- [34] Kiefera R, Temmer R, Tamm T, Travas-Sejdic J, Kilmartin PA, Aabloo A. Conducting polymer actuators formed on MWCNT and PEDOT-PSS conductive coatings. *Synthetic Metals*. 2013;**171**:69-75. DOI: 10.1016/j.synthmet.2013.03.017
- [35] Koidis C, Logothetidis S, Kapnopoulos C, Karagiannidis PG, Laskarakis A, Hastas NA. Substrate treatment and drying conditions effect on the properties of roll-to-roll gravure printed PEDOTPSS thin films. *Materials Science and Engineering B*. 2011;**176**:1556-1561. DOI: 10.1016/j.mseb.2011.03.007

- [36] Jin Y, Li Q, Chen M, Li G, Zhao Y, Xiao X, Wang J, Jiang K, Fan S. Large area nanoscale metal meshes for use as transparent conductive layers. *Nanoscale*. 2015;**7**:16508-16515. DOI: 10.1039/c5nr04528b
- [37] Sun T, Akinoglu EM, Guo C, Paudel T, Gao J, Wang Y, Giersig M, Ren Z, Kempa K. Enhanced broad-band extraordinary optical transmission through subwavelength perforated metallic films on strongly polarizable substrates. *Applied Physics Letters*. 2013;**102**:101114. DOI: 10.1063/1.4795151
- [38] Mizuno K, Ishii J, Kishida H, Hayamizu Y, Yasuda S, Futaba DN, Yumur M, Hata K. A black body absorber from vertically aligned single-walled carbon nanotubes. *PNAS*. 2009;**106**:6044-6047. DOI: 10.1073/pnas.0900155106
- [39] Fotea C, Callaway J, Alexander MR. Characterisation of the surface chemistry of magnesium exposed to the ambient atmosphere. *Surface and Interface Analysis*. 2006;**38**: 1363-1371. DOI: 10.1002/sia.2463

